108, 1402 (1957).
[21]D. G. Thomas, M. Gershenzon, and J. J. Hopfield, Phys. Rev. 131, 2397 (1963).
[22]W. G. Spitzer, M. Gershenzon, C. J. Frosh, and D. F. Gibbs, J. Phys. Chem. Solids 11, 339 (1959).
[23]A. D. Remenyuk, L. G. Zabelina, Yu. I. Ukhanov, V. M. Tuchkevich, and Yu. V. Shmartsev, in *Proceedings of the Ninth International Conference on the Physics of Semiconductors, Moscow*, 1968, edited by S. M. Rykin and Yu. V. Shmartsev (Nauka, Leningrad, 1968).
[24]R. Zallen and W. Paul, Phys. Rev. 134, A1628 (1964).

PHYSICAL REVIEW B VOLUME 5, NUMBER 8 15 APRIL 1972

Pressure Dependence of the Carrier Concentrations in p-Type Alloys of $Hg_{1-x}Cd_xTe$ at 4.2 and 77 °K*

C. T. Elliott,† John Melngailis, T. C. Harman, J. A. Kafalas, and W. C. Kernan
Lincoln Laboratory, Massachusetts Institute of Technology, Lexington, Massachusetts 02173
(Received 6 December 1971)

Electrical transport measurements have been made on p-type samples of $Hg_{1-x}Cd_xTe$ with x near 0.15 at temperatures of 4.2 and 77 °K and at hydrostatic pressures up to 9 kbar. A sharp transition is observed in both the Hall coefficient and conductivity versus pressure at 4.2 °K. The pressure dependence of the carrier concentrations and mobilities has been obtained from magneto-Hall and magnetoresistance data. Analysis using $\vec{k}\cdot\vec{p}$ theory yields values for the Fermi energy, measured with respect to the valence-band edge, of more than 9 meV, which are independent of pressure. A possible model to account for this behavior is described. Magnetic freeze-out effects have been observed and attributed to the lowest-energy, spin-split, zero-order Landau level passing through the Fermi energy. A value of 7×10^{-6} eV/bar is obtained for the pressure coefficient of the energy gap at 77 °K. Non-Ohmic behavior has been observed at 4.2 °K during the magnetic freeze-out.

INTRODUCTION

A continuous range of $Hg_{1-x}Cd_xTe$ alloys can be formed between the semimetal HgTe and the semiconductor CdTe. The general features of the band structure are now well established (see review papers by Long and Schmit[1] and Harman[2]). HgTe is a semimetal with an inverted band structure, like that proposed for gray tin,[3] with a negative Γ_6-Γ_8 energy gap of 0.3 eV, at low temperature. The energy gap increases approximately linearly with x, going through zero for $x\simeq0.15$ at low temperature. At higher values of x the alloys are semiconducting with a band structure qualitatively like that of the direct-gap III-V compounds. A large number of investigations (see review papers for references) have established that the dispersion relation for the conduction band is well described by Kane's $\vec{k}\cdot\vec{p}$ model.[4] A recent determination[5] from magnetoreflection measurements yielded a value of 8.4×10^{-8} eV cm for the Kane matrix element.

The behavior of n-type $Hg_{1-x}Cd_xTe$ is now relatively well understood, but the valence-band parameters have yet to be established. Reported values for the heavy-hole mass range from $0.3m_0$ to $7m_0$,[5-11] and the band overlap energy in the semimetallic alloys, due to the warping of the heavy-hole band, has not been reliably determined. In general, the electrical transport properties of the p-type alloys have proved complex and difficult to interpret.[5,12-14]

The object of this work was to obtain information on the valence-band structure and on acceptor levels near the valence-band edge. Measurements of the electron and hole concentrations have been made on p-type, nearly zero-band-gap semiconducting samples, as the energy gap was opened up with hydrostatic pressure. Because of the high electron-to-hole mobility ratio the minority electrons can dominate the transport properties in the semimetallic state and large changes in the transport coefficients occur during the semimetal-semiconductor transition produced by applying pressure.

Hydrostatic pressure measurements have been made previously only on n-type $Hg_{1-x}Cd_xTe$[15] and HgTe[16,17] at 300 and 77 °K, and on p-n junctions in $Hg_{1-x}Cd_xTe$.[18] The values obtained for the pressure coefficient of the energy gap vary from 8 to 14×10^{-6} eV/bar.

In this paper we describe first the experimental procedure, then the results obtained, and finally the analysis and interpretation of the results.

EXPERIMENTAL PROCEDURE

Sample Preparation

Single crystals of $Hg_{1-x}Cd_xTe$ were grown by a

new technique[19] which is believed to involve mass-transport-induced growth and simultaneous temperature-gradient annealing in a vertical ampoule 1.8 cm in diameter.

The composition x of the ingot was a function of distance along the growth direction. Slices were cut from the ingot perpendicular to the growth direction and etch polished to a thickness of about 0.50 mm. The composition x within a slice was found to be constant within the accuracy of the electron microprobe ($\Delta x = \pm 0.005$). The slices were further cut into rectangular parallelepiped wafers $1.2 \times 0.4 \times 0.05$ cm.

The samples that we will report on are from three wafers: 7B with $x = 0.149$, 7B1 with $x = 0.149$, and 8B with $x = 0.138$. The latter two were used unannealed. To reduce the acceptor concentration, wafer 7B (thickness 0.3 mm) was annealed for four days at 400 °C in Hg vapor. It was verified to be homogeneous in carrier concentration by Hall measurements on a sample progressively thinned by etching. (The unannealed wafers, cut from a large crystal, are expected to be homogeneous in thickness. Several small samples cut from each wafer showed the same carrier concentration within the accuracy of about 10% of the measurement of the Hall constant.)

Unoriented single-crystal samples, typically of dimensions $3.0 \times 0.7 \times 0.3$ mm, were cut from the wafers with a 0.005-in. nichrome-wire saw using a Carborundum-oil slurry.

Just before etching, the samples were rinsed for three minutes in turn in hot xylene, in acetone, and in hot methyl alcohol. The samples were not exposed to air but were left in the bottom of a beaker covered by a small amount of methyl alcohol. The etchant consisting of 20% bromine and 80% methyl alcohol (by volume) was poured into the beaker and agitated. The etching was stopped after about 10 sec by pouring a large quantity of methyl alcohol into the beaker. The usual, more dilute, Br-methanol etches can yield conducting surface layers, which have been observed at 4.2 °K on larger-gap semiconducting, p-type $Hg_{0.70}Cd_{0.30}Te$. The above etch[20] left no detectable conducting layer on $Hg_{0.70}Cd_{0.30}Te$ samples with resistivities as high as $10^5\ \Omega$ cm.[21] Since the resistivity of the samples discussed here was always below $10^3\ \Omega$ cm, the surface conduction left by the etching should be insignificant.

Six contacts were made to the samples by electroplating gold and then indium, as follows: The samples were held down on a microscope slide by the sharp tip of a spring-loaded tungsten wire, and the sample and most of the wire were covered by microstop (a red lacquer). When it was dry, 0.02-cm strips were cut in the microstop on the glass. These strips terminated at the sample and were peeled off, exposing the parts to be plated. Using the tungsten wire to make electrical contact, a thin layer of gold followed by a thicker layer of indium was plated on. Gold wires (0.001-in. diam) were indium soldered to the plated regions. These contacts were able to withstand the temperature and pressure cycling involved in the experiments.

Measurements

The samples were mounted in a Be-Cu pressure bomb (1.43-cm o.d., 0.32-cm i.d.), which, when pumped to the desired He-gas pressure (0–9 kbar), could be lowered into a Dewar. The Hall and resistivity voltages were displayed on an xy recorder as a function of magnetic field. (The sample mounting and pressure techniques have been described in more detail in Ref. 22.)

For the 4.2 °K measurements the bomb was slowly lowered into the Dewar, so that the pressurized helium solidified from the bottom up. There may be some uncertainty about the final pressure in the bomb. For example, helium at 8 kbar solidifies at 55 °K.[23,24] If it then cools to 4.2 °K at constant volume, the pressure would drop by about 8%. Most of this drop, however, occurs in the first 15 °K of cooling. Differences in temperature between the two ends of the bomb cavity (length 10 cm) during the cooling are expected to be higher than 15 °K. Therefore, assuming that within the bomb cavity solid helium cannot support a pressure gradient,[24,25] a large portion of the pressurized helium in the bomb cools through the first 15 °K after solidification at constant pressure. When the helium in the 0.050-cm-i.d. pressure tubing, which is connected to the top of the bomb, finally solidifies, the bomb becomes effectively sealed and the rest of the cooling takes place at constant volume. In the following we assume that the pressure in the bomb at 4.2 °K is the externally maintained pressure. In view of the above considerations, this is thought to be closer to fact than the assumption of cooling at constant volume.[25]

RESULTS AND PRELIMINARY ANALYSIS

Figures 1 and 2 show the zero-field resistivity and low-field Hall coefficient as a function of pressure for the three samples at 4.2 °K. A clear transition is indicated by the sharp rise in resistivity and the sudden change of sign of the Hall coefficient, which results from the removal of the minority electrons. For samples 7B and 7B1 the transition occurs between 3 and 4 kbar, and for sample 8B between 7 and 8 kbar. In sample 7B (annealed sample), the resistivity increases by more than three orders of magnitude, indicating that only a small fraction of the conductivity at atmospheric pressure is due to holes.

In order to obtain the concentrations and mobil-

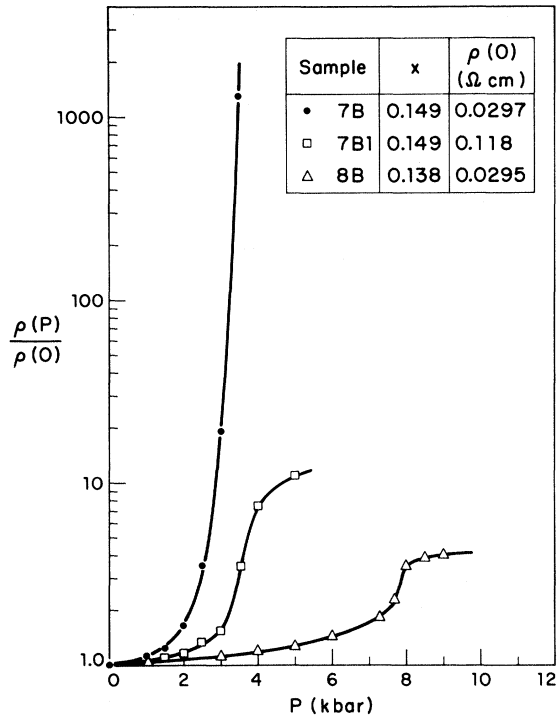

FIG. 1. Values of the relative resistivity as a function of pressure at 4.2 °K. The inset shows the composition of the samples and the resistivity at atmospheric pressure.

ities of electrons and holes in the samples as a function of pressure, the magnetic field dependence of the Hall coefficient and the conductivity were measured at a set of pressures. These measurements were made at both 77 and 4.2 °K. Examples of the results obtained at 77 °K are shown in Figs. 3 and 4. Data of this type are frequently analyzed by using multiband expressions for R and ρ to obtain a least-squares fit.[26,27] We believe that this procedure is not applicable in the present case, since it is based on the implicit assumption that the concentration of holes and electrons is independent of magnetic field. This assumption is not valid for electrons at 4.2 °K (and probably not valid at 77 °K), since, owing to the pinned Fermi level and the small electron effective mass, the lowest Landau level passes through the Fermi level. Over most of the pressure range used for our measurements, the position of the Fermi level in the samples is fixed relative to the valence-band edge by the high hole concentrations, and a magnetic field reduces the electron concentration by changing the density-of-states distribution in the conduction band. In sample 7B at 77 °K, for example, $\mu_n B$ is greater than unity even in magnetic fields smaller than 1 kG, and the electron-Landau-level separation may be comparable with kT in fields less than 10 kG. We return to this point below in discussing longitudinal magnetoresistance effects.

In some cases the carrier concentrations and mobilities at zero field can be obtained by a method that employs only the low-field and strong-field values measured for the Hall coefficient and conductivity. This method, which is outlined in the Appendix, was used to analyze the data for sample 7B at 77 °K.

The electron concentration and mobility of sample 7B as a function of pressure are shown in Figs. 5 and 6. The maximum magnetic field available for the measurements on this sample was 25 kG, and saturation of the positive Hall coefficient was only observed at 4 kbar and higher pressures. Above 4 kbar, the hole concentration and mobility were constant at 1.5×10^{16} cm^{-3} and 450 cm^{2}V^{-1} sec^{-1}, respectively. The electron concentration can be obtained for pressures below 4 kbar since $\sigma_n \gg \sigma_p$ and $n = 1/R(0)e$ (see the Appendix). The dashed lines in Figs. 3 and 4 for sample 7B at 7.5 kbar were computed using a two-band expression for R, which assumes energy-independent relaxation times for both carriers, and the zero-field carrier concentrations and mobilities for this pressure, obtained from the analysis. The change in sign of R occurs experimentally at a lower magnetic field than the one given by the calculated curve. This discrepancy is consistent with a decrease in electron concentration with increasing magnetic field.

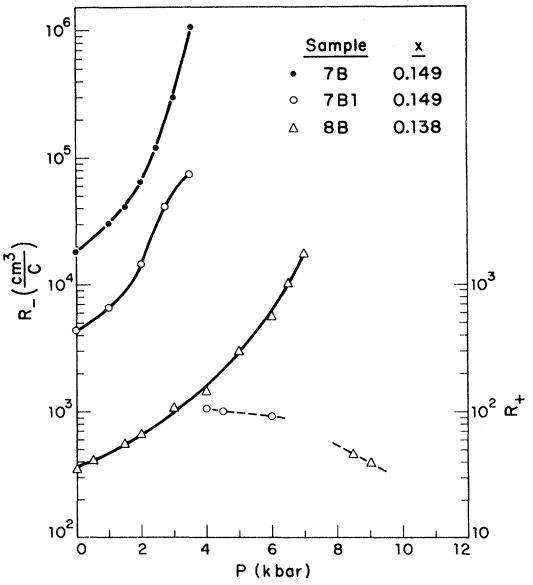

FIG. 2. Low-field Hall coefficient R as a function of pressure at 4.2 °K. The solid lines indicate negative values of R (left scale) and the dashed lines positive values (right scale).

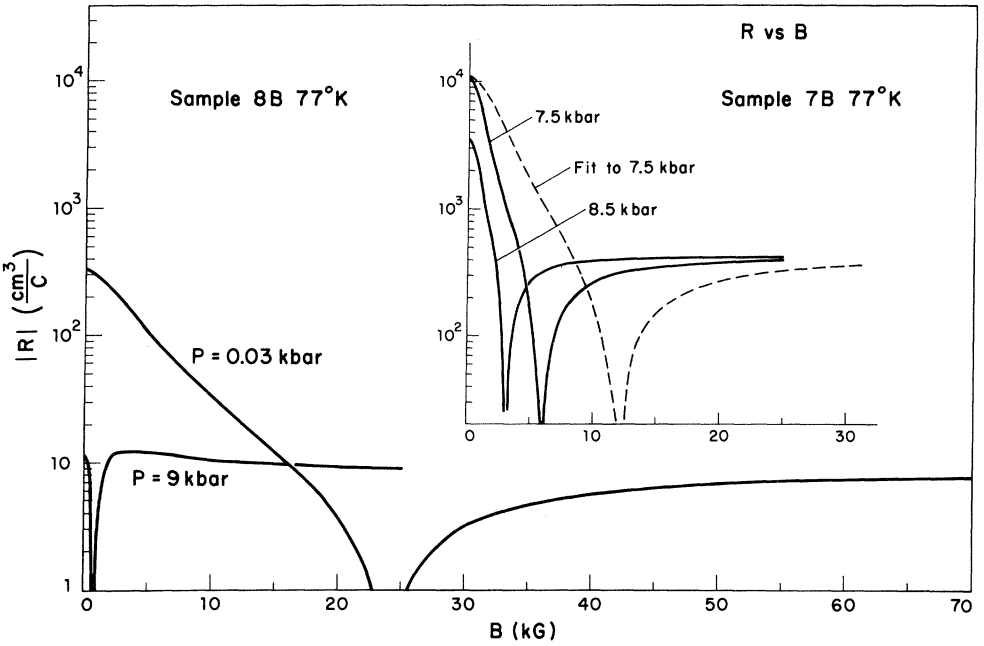

FIG. 3. Hall coefficient R as a function of magnetic field in samples 8B and 7B at 77°K. R is negative for low fields and changes sign with increasing field. The fitted curve (dashed) represents the usual two-carrier expression for R with the two-carrier densities and two mobilities obtained by making the Hall coefficient and conductivity agree at $B=0$ and $B=\infty$. The lack of agreement in the crossover region is due to quantum effects (see text).

For the as-grown samples 7B1 and 8B the hole concentrations at 77 °K, determined from the saturation value of R, are much higher and decrease by approximately 20% with pressure from 0 to 9 kbar. In these two samples the ratio $\sigma_p(0)/\sigma_n(0)$ becomes large at quite low pressures, and the analysis of the Appendix becomes inaccurate. The electron concentration and mobility at 77 °K have therefore been obtained only at zero pressure. The results for all three samples at $P=0$ are summarized in Table I.

Figure 7 shows some examples of the Hall coefficients vs magnetic field curves obtained at 4.2 °K. For sample 7B at low pressure (0.03

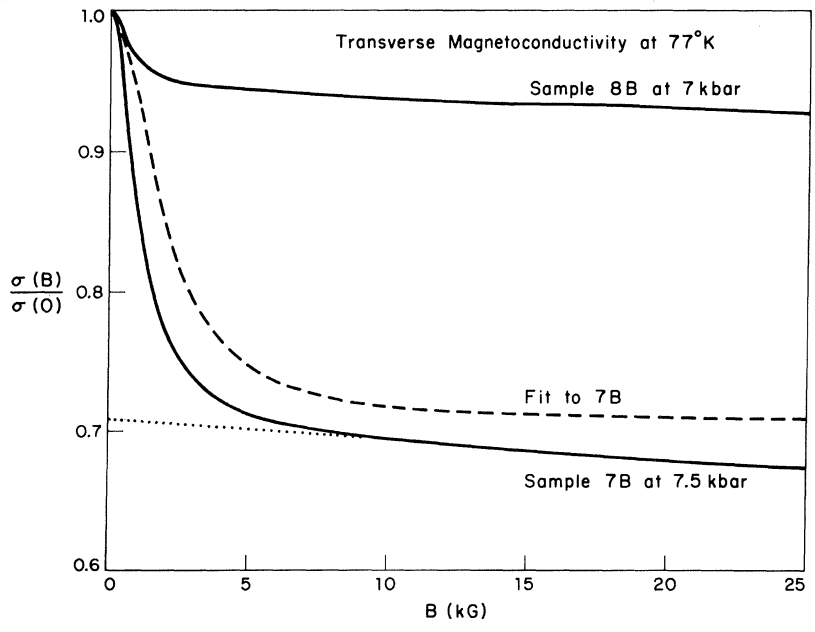

FIG. 4. Transverse magnetoconductivity as a function of magnetic field for samples 7B and 8B at 77°K. The steady decrease in the conductivity at higher fields is believed to be due to geometric effects. (The sample width is approximately one-half the voltage-contact spacing, and about one-fourth of the sample length.) The asymptotic value of $\sigma(\infty)/\sigma(0)$ was found by extrapolating the experimental curve back to zero field (dotted straight line).

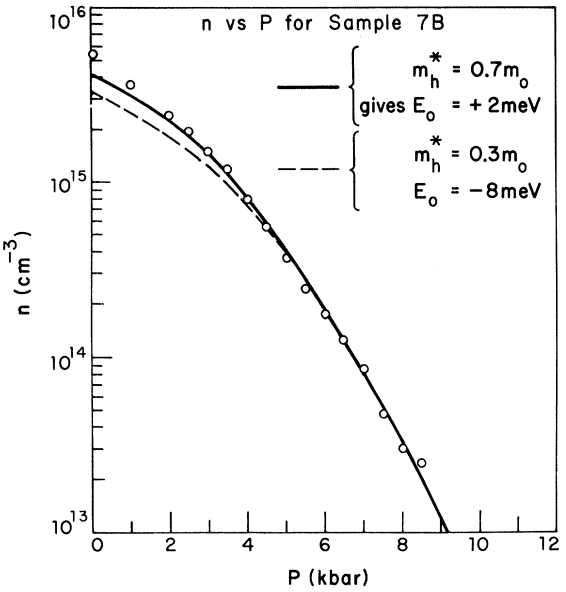

FIG. 5. Number of electrons in sample 7B as a function of pressure. The points are the values of n deduced from the experimental data. The lines are calculated from the Kane's $\vec{k}\cdot\vec{p}$ model with $P_K = 8.4\times10^{-8}$ eV/cm, $\alpha = dE_g/dP = 7.0\times10^{-6}$ eV/bar.

kbar), R is constant initially and then shows strong quantum effects but remains negative. The resistivity rises very rapidly with transverse magnetic field from 0.03 Ω cm to more than 80 Ω cm at 20 kG. At high fields the Hall angle was less

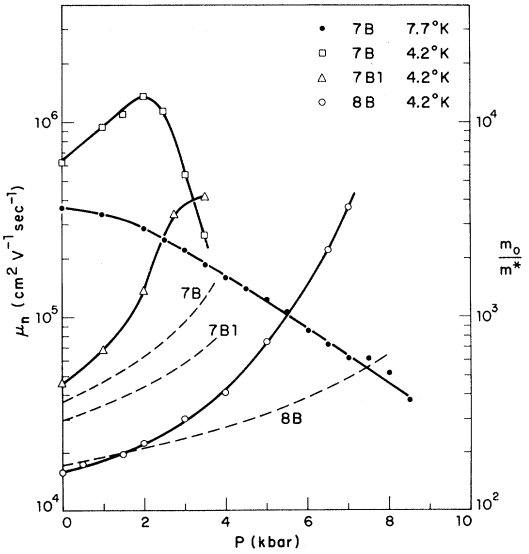

FIG. 6. Electron mobility as a function of pressure for the three samples. The variation of the reciprocal effective mass due to the change in E_g is shown by the dashed lines for comparison. The mobility is seen to increase faster than $1/m^*$ at low pressure, and for sample 7B at 4.2 °K to turn downward above 2 kbar.

TABLE I. Values for the carrier concentrations and mobilities at atmospheric pressure.

		77 °K			$P=0$	4.2 °K		$P=0$	
Sample	x	p (cm^{-3})	μ_p (cm^{2}V^{-1} sec^{-1})	n (cm^{-3})	μ_n (cm^{2}V^{-1}sec^{-1})	p (cm^{-3})	μ_p (cm^{2}V^{-1}sec^{-1})	n (cm^{-3})	μ_n (cm^{2}V^{-1}sec^{-1})
7B	0.149 ± 0.005	1.5×10^{16} ($P>5$ kbar)	450 ($P>5$ kbar)	5.3×10^{15}	3.7×10^5	...	...	3.4×10^{14}	6.3×10^5
7B1	0.149 ± 0.005	6.3×10^{17}	174	3.0×10^{15}	3.2×10^4	1.5×10^{17}	76	8.8×10^{14}	4.6×10^4
8B	0.138 ± 0.005	8.3×10^{17}	168	4.8×10^{15}	2.5×10^4	7.6×10^{17}	78	3.2×10^{15}	1.6×10^4

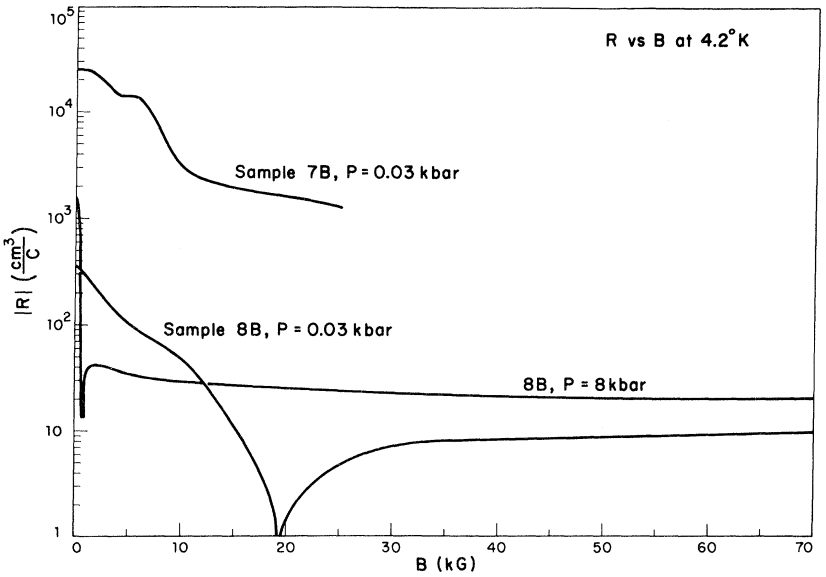

FIG. 7. Measured Hall coefficient vs magnetic field for samples 7B and 8B. R_H is negative for 7B and at low fields for 8B. The structure in the curve for sample 7B is thought to be due to quantum effects.

than 5×10^{-4} rad and we were unable to determine R owing to contact misalignment. For sample 8B at 8 kbar, the positive Hall coefficient decreases with magnetic field, falling to a value of approximately one-half its maximum value at 1.5 kG. Similar behavior was observed at 77 °K for samples 7B1 and 8B, but not for 7B, where the positive R was independent of magnetic field. The values for p quoted in Table I are obtained from the limiting value of R in strong fields.

The electron concentration and mobility for sample 7B at 4.2 °K have been obtained directly from $R(0)$ and $\sigma(0)$ since $\sigma_n(0) \gg \sigma_p(0)$, while the carrier concentrations and mobilities for samples 7B1 and 8B were obtained by using the method of the Appendix. The electron concentrations and mobilities for all three samples are shown as a function of pressure in Figs. 6 and 8. The hole concentrations and mobilities for sample 7B1 and 8B at zero pressure are given in Table I. The hole concentrations fall by approximately 40% between 0 and 9 kbar.

Longitudinal magnetoconductivity measurements were made on all three samples at helium temperatures at a series of fixed pressures. Some typical results are shown in Fig. 9. Shubnikov–de Haas oscillations were observed in many cases in the low-field region; see, for example, the $P=0$ curve of Fig. 9(b). The oscillations were observed for sample 8B at pressures up to 5 kbar [although they cannot be seen on the compressed scale of Fig. 9(a)]. The electron concentrations obtained from the periods of the oscillations in this sample are plotted in Fig. 8. These electron concentrations obtained at zero pressure for samples 7B and 7B1 are in good agreement with the concentrations obtained from the Hall data. Measurements were made on sample 8B at 77 °K, and here the conductivity was observed to change by a factor of 2 at low pressures, the change occurring

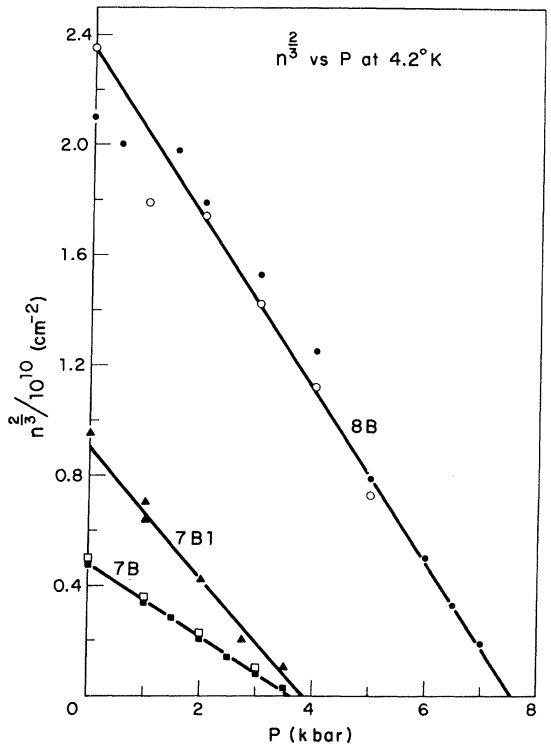

FIG. 8. Plot of the $\frac{2}{3}$ power of the electron concentration vs pressure at 4.2 °K for the three samples. The straight lines are calculated from the $\vec{k}\cdot\vec{p}$ theory. The open and solid squares for sample 7B indicate the results from two specimens. For sample 8B the open circles represent $n^{2/3}$ deduced from Shubnikov–de Haas results and the solid circles from Hall data.

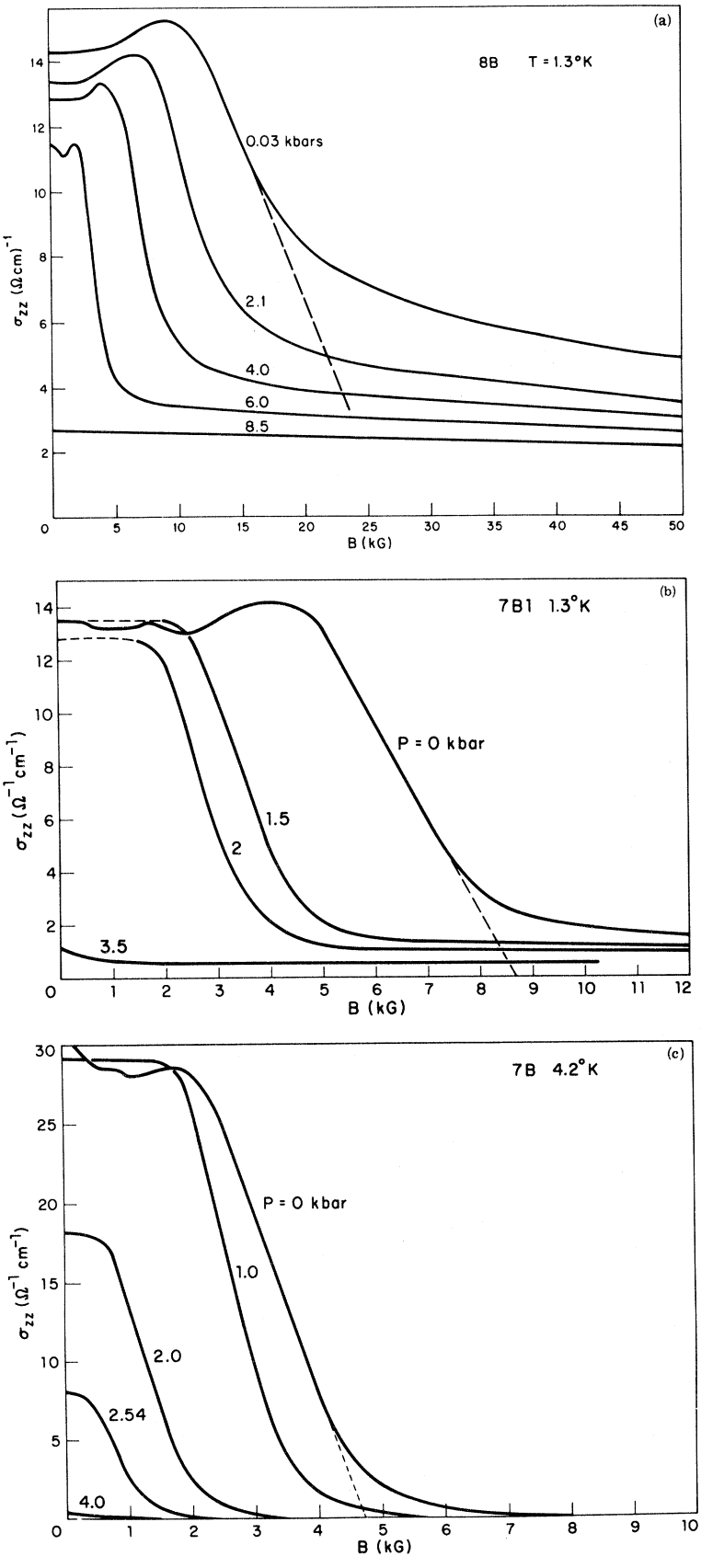

FIG. 9. (a) Longitudinal magnetoconductivity of sample 8B at 1.3 °K as a function of magnetic field for several pressures. The straight portion of the dropoff is fitted to an expression derived from Kubo, Miyake, and Hashitsume (Ref. 35) (shown dashed). (b) Longitudinal magnetoconductivity of sample 7B1 at 1.3 °K. Shubnikov–de Haas oscillations, which are not readily visible on this scale, are present in the dashed portion of the curves at low fields. (c) Longitudinal magnetoconductivity of sample 7B at 4.2 °K.

more slowly with magnetic field than at helium temperatures.

Non-Ohmic behavior of sample 7B was observed at helium temperatures and at pressures up to 4 kbar. This could be seen on I-V plots at various magnetic fields. But more features can be seen on the V-B curves shown in Fig. 10, which is a photograph of the direct recorder traces of the voltage drop (or electric field) along the sample as a function of magnetic field at various constant currents. At currents below 1 mA the resistivity rises smoothly with magnetic field. At higher currents it rises more slowly and in particular shows a slight "knee" or discontinuity in slope. In Fig. 10 the positions of the knees are seen to fall on a straight line on the plot of electric field vs magnetic field. The top portion of Fig. 10 shows a plot of the derivative vs magnetic field of the 2-mA curve. In addition to the "knee" other structure with a complicated current dependence is observed. At 1 mA no corresponding structure (or knee) in the derivative could be detected. At present we do not understand this behavior.

ANALYSIS USING $\vec{k}\cdot\vec{p}$ MODEL

The observed variation of the electron concentration with pressure P results from the pressure dependence of the energy gap E_g. We have fitted the n-vs-P curve for sample 7B at 77 °K (Fig. 5) by assuming a linear pressure dependence:

$$E_g = E_0 + \alpha P \quad ,$$

where E_0 is the energy gap at zero pressure, α the pressure coefficient of E_g, and P the applied pressure. A similar method has been used by Schmit[28] to calculate the intrinsic concentration in $Hg_{1-x}Cd_xTe$ alloys.

The concentration of ionized acceptors, N_A', was assumed to be independent of pressure, and equal to 1.5×10^{16} cm^{-3}, the value of p determined from the limiting value of R at high pressure. The position of the Fermi level was adjusted at each pressure until the calculated values of n and p satisfied the condition

$$p - n = N_A' \quad .$$

The electron concentration was obtained by numerical integration of an expression given by Harman and Strauss[29] which is based on the Kane model and includes the effects of nonparabolicity and statistical degeneracy. A value of[5] 8.4×10^{-8} eV cm was used for the Kane matrix element. The valence band was assumed to be parabolic with an effective mass m_v^* and the hole concentration was obtained using the standard density-of-states expression. The calculations were made for masses between $0.3m_0$ and $0.7m_0$, the range of values reported for m_v^* in $Hg_{1-x}Cd_xTe$ and HgTe.[5-11]

The values of E_0 and α were adjusted to fit the calculated curve of n vs P to the experimental curve. The curve obtained for the two extreme values of m_v^* are shown in Fig. 5. The pressure coefficient in both cases is 7.0×10^{-3} eV/kbar and the values for E_0 are +2 and −8 meV for m_v^* of $0.7m_0$ and $0.3m_0$, respectively. These may be compared with values of +11.6 and −15 meV obtained for $x=0.15$ from empirical expressions for $E_g(x, T)$ given by Wiley and Dexter[8] and Scott,[30] respectively. The behavior of the electron mobility shown in Fig. 6 is consistent with $E_g=0$ near $P=0$. The failure to fit the experimental n-vs-P data well at low pressures may be due to an incorrect choice of m_v^* or to the invalidity of the assumption that N_A' is constant. The latter will be strictly true only if the acceptor ionization energy is small relative to kT, and the analysis below indicates that the acceptor energy in this sample is comparable with kT at 77 °K. At higher pressure where $N_A' \gg n$, the slope in Fig. 5 is sensitive to the pressure coefficient, and relatively insensitive to the other parameters. The fitting at 77 °K should therefore yield a reliable value for α.

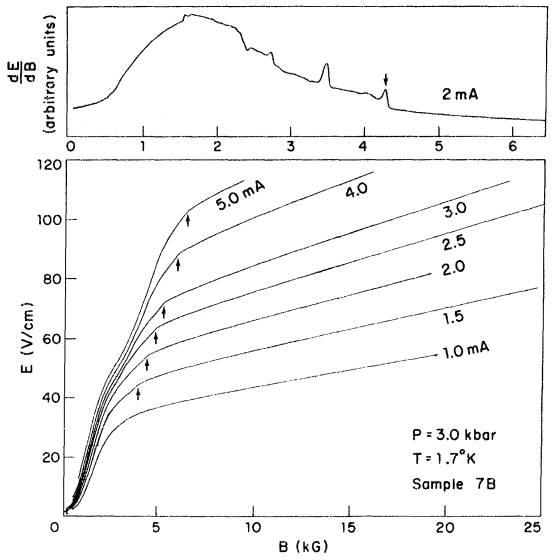

FIG. 10. Photograph of the direct recorder traces of the voltage drop (or electric field) along sample 7B as a function of magnetic field for several currents. (The sample cross-sectional area is 2.5×10^{-3} cm^2.) The sample is non-Ohmic, since for $B>5$ kG, E is not proportional to the current. In addition, structure is observed in the region $1.5<B<6$ kG for sample currents greater than 1 mA. This structure is shown on an expanded scale by the derivative curve in the upper part of the figure. "Knees" appear in the curves at fields (4.25 kG on the 2-mA curve) which mark a disappearance of the structure. These "knees" marked by arrows are seen to fall on a straight line on the E-vs-B plot.

The analysis of the data obtained at helium temperatures is considerably simplified by the assumption of strong statistical degeneracy. An expression for the electron concentration is obtained as follows. For a spherically symmetrical conduction band the electron concentration is given by

$$n = k_F^3/3\pi^2 \ , \tag{1}$$

where k_F is the electron wave vector at the Fermi surface.

The $E(\vec{k})$ relationship for the conduction band from $\vec{k}\cdot\vec{p}$ theory for the case of kP_K and E_g very much less than the spin-orbit splitting energy is[4]

$$E(k) = \frac{\hbar^2 k^2}{2m_0} + \frac{E_g + (E_g^2 + \frac{8}{3}k^2P_K^2)^{1/2}}{2} \ , \tag{2}$$

where P_K is the Kane matrix element, and the energies are measured from the valence-band edge. The first term is negligible for the narrow-gap alloys. By replacing $E(k)$ and k by their values at the Fermi level, E_F and k_F, and rearranging, we obtain (for $E_F > E_g$)

$$k_F^2 = \frac{3}{2P_K^2} E_F (E_F - E_g) \ . \tag{3}$$

Combining Eqs. (1) and (3) yields

$$n^{2/3} = \left(\frac{1}{3\pi^2}\right)^{2/3} \frac{3}{2P_K^2} E_F(E_F - E_g) \ . \tag{4}$$

On substituting $E_g = E_0 + \alpha P$ this becomes

$$n^{2/3} = \left(\frac{1}{3\pi^2}\right)^{2/3} \frac{3}{2P_K^2} E_F(E_F - E_0 - \alpha P) \ . \tag{5}$$

The expression is valid in both the normal- and inverted-band-structure regions, provided that the correct sign is used for E_0 (E_0 is negative for the inverted band structure).

The electron concentrations obtained experimentally at 4.2 °K for the three samples are shown in Fig. 8, plotted as $n^{2/3}$ vs P. A straight line is obtained in each case, indicating that the position of the Fermi energy relative to the valence-band edge is independent of pressure. The slope of the line yields $\alpha E_F/P_K^2$. E_F is found by taking $\alpha = 7\times10^{-3}$ eV/kbar (the value obtained at 77 °K) and $P_K = 8.4\times10^{-8}$ eV cm.[5] E_0 is then obtained from E_F and the intercept on the pressure axis. The values of E_F and E_0 found in this way are given in Table II. The small difference in E_0 for samples 7B1 and 7B, which were taken from the same slice of the parent crystal, could be due to an undetected difference in alloy composition. The required difference in x is 0.004, which is within the experimental error of the microprobe analysis. Values for E_0 calculated for the measured values of x from empirical expressions[8,30] for $E_g(x, T)$ are also listed in Table II. Those obtained from the expression given by Wiley and Dexter,[8] which assumes a linear dependence of energy gap on both composition and temperature, agree well with the experimental values.

DISCUSSION

According to the $\vec{k}\cdot\vec{p}$ analysis, at 4.2 °K the position of the Fermi level, with respect to the valence band, is independent of pressure in all three samples. It is situated more than 9 meV (or $25kT$) above the conduction-band edge at zero pressure. This must be reconciled with hole concentrations greater than 10^{17} cm^{-3} which are measured in samples 7B1 and 8B at 4.2 °K. The high values for the np product cannot be due to an overlap of the conduction and valence bands, since the high hole density is not observed in sample 7B.

A possible model to account for the observed behavior is shown in Fig. 11. The energy-band structure near the zone center is shown as a function of pressure for an alloy which is semimetallic at zero pressure. We show an acceptor level situated above the heavy-mass valence-band edge, whose energy with respect to the valence-band edge does not change with pressure. Thus, below the pressure P_c the acceptor states lie within the conduction band. Evidence for discrete impurity states lying within a band of states has been obtained in other materials. In CdTe the

TABLE II. Values at 4.2 and 77 °K for the energy gap at zero pressure and the Fermi energy.

Sample	T (°K)	x	E_F (meV)	E_0 (meV)	E_0 calculated (meV) (Ref. 8)	E_0 calculated (meV) (Ref. 30)
7B	4.2	0.149 ± 0.005	9	−16	−14 ± 9	−45 ± 9
7B1	4.2	0.149 ± 0.005	16	−10	−14 ± 9	−45 ± 9
8B	4.2	0.138 ± 0.005	20	−33	−35 ± 9	−63 ± 9
7B	77	0.149 ± 0.005	23[a]	−8.0	+11.6	−15
			31[b]	+2.0	+11.6	−15

[a]Calculated assuming a hole mass $m_h^* = 0.3$

[b]Hole mass $m_h^* = 0.7$.

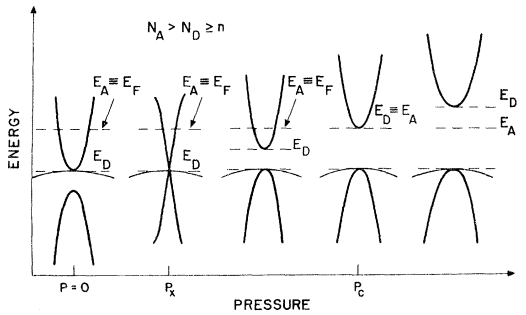

FIG. 11. Schematic of the band structure of $Hg_{1-x}Cd_xTe$ at the zone center as a function of pressure. N_A and N_D are the densities of acceptors and donors, respectively. The electron density n is $\int_{E_c}^{E_f} g(E)dE$, where $g(E)$ is the density of states in the conduction band and E_c the energy at the band edge.

donor states associated with Ga, In, Cl, and Br are believed to lie above the Γ_6 minimum[31] and in $GaAs_{1-x}P_x$:N a resonant state of the N isoelectric trap has been shown to exist above the conduction-band minimum for $x = 0.19$ and 0.21.[32]

To explain the results for sample 7B, we assume that this sample is compensated with a donor density which is greater than the number of conduction-band states below the acceptor level (but less than the density of acceptor states). The donor level is at the bottom of the conduction band. In this situation the Fermi energy is pinned at the acceptor level. With applied pressure the electron concentration falls as the number of states below E_A decreases and becomes zero at a pressure P_c, where E_g is equal to E_A. The value for E_A from Table II is 9 meV.

We suggest that in samples 7B1 and 8B the acceptor density is high enough to form a band of states in which "metallic" impurity-band conduction[33] takes place. The holelike conduction observed at low temperatures is now attributed to this band and not the valence band. The Fermi energy is within the impurity band and the electron concentration in the conduction band will be zero at a pressure P_c for which E_g is equal to E_F. The values for the hole mobility at 4.2 °K of 76 and 78 $cm^2V^{-1}sec^{-1}$ (Table II) are typical of the magnitude obtained for this type of impurity-band conduction. This is not necessarily evidence for the model, however, since similar values would be expected for valence-band holes due to ionized impurity scattering at these impurity concentrations.

Other evidence for acceptor energies in the range 10–25 meV has been obtained for $Hg_{1-x}Cd_x$ Te, with x near 0.3, from Hall-effect and photoluminescence measurements.[13] Also, an unexplained line in the magnetoreflection data of Groves, Harman, and Pidgeon[5] would be consistent with a level situated approximately 20 meV above the valence-band edge.

The relatively low values for the electron mobility for samples 7B1 and 8B (Fig. 6) might also be expected since electrons at the Fermi surface can be scattered into the acceptor band states. We have not attempted an analysis of the pressure dependence of the mobility. We simply show in Fig. 6 the variation of $1/m_{eF}^*$ with pressure for the three samples, calculated using the values for E_0 and E_F given in Table II, where m_{eF}^* is the electron effective mass at the Fermi level. The electron effective mass is given by $m_e^* = \hbar^2 k(dE/dk)^{-1}$. Using the dispersion relation of Eq. (2) and k_F from Eq. (3), we obtain

$$\frac{m_0}{m_{eF}^*} = 1 + \frac{4P_K^2}{3\hbar^2} m_0(E_g - 2E_F)^{-1} \quad . \tag{6}$$

It is apparent from Fig. 6 that the mobility variations cannot be accounted for by changes in the electron mass alone. The mobility for samples 7B1 and 8B varies more rapidly with pressure than $1/m_{eF}^*$, and the mobility for sample 7B shows a maximum which is not exhibited by $1/m_{eF}^*$.

The carrier concentrations in sample 7B at 77 °K are fitted quite well by the values calculated by using the Kane model (Fig. 5). However, the np products for samples 7B1 and 8B at 77 °K and zero pressure (Table I) are very high. Calculations using estimated values for E_0 yield values for np an order of magnitude lower than those obtained from the experimental values. We speculate that this is also due to the presence of an impurity band, the major part of the hole conduction in the samples occurring in the impurity band rather than the valence band. The presence of some valence-band conduction would account for the higher hole mobilities relative to the 4.2 °K values.

Measurements of the Hall coefficient at higher pressures, where the electron concentration is low, on samples 7B1 and 8B show a positive R falling with magnetic field initially (Figs. 3 and 7). This behavior can be accounted for by the presence of two sets of holes of different mobility, but to fit the magnetic field dependence the higher mobility set are required to have a mobility of order 10^4 $cm^2V^{-1}sec^{-1}$. One explanation[34] would be that the high mobility carriers are in the light-mass valence band, but since the positive Hall coefficient in sample 7B does not show the same behavior, we think that it is not correct.

The behavior of the longitudinal magnetoconductivity shown in Fig. 9 can also be explained using the model shown in Fig. 11. The conductivity is made up of two components which can be regarded as independent in this geometry: σ_{zz}^e due to electrons and σ_{zz}^h due to holes. At high pressures where the electron concentration is very small, $\sigma_{zz} \simeq \sigma_{zz}^h$

and shows only a small magnetic field dependence. At low pressures and zero magnetic field the conductivity is much higher because of the electronic contribution. With applied magnetic field, oscillatory behavior is first observed as the Landau levels pass through the Fermi energy. The rapid fall in conductivity at higher fields (over more than three orders of magnitude for sample 7B) we attribute to the fall in electron concentration and electron mobility as the last Landau level approaches and passes through the Fermi energy. Kubo, Miyake, and Hashitsume[35] have obtained expressions for the transport coefficients in the quantum limit. The following expression for the longitudinal magnetoconductivity, for the case of the Fermi energy independent of magnetic field, is derived from Eqs. 13–34 of Ref. 35 using Eqs. 8-14 and 12-7 of the same reference (the expression is valid for parabolic bands, and we neglect collision broadening):

$$\sigma_{xx}^{e}=\frac{2e^2\hbar}{\pi W m^*}\left(\phi-\tfrac{1}{2}\hbar\omega\right) \quad , \tag{7}$$

where ϕ is the Fermi energy measured from the conduction-band edge and ω is the cyclotron frequency eB/m^*c. W is a constant defined as $W=n_s[(2\pi\hbar^2/m^*)f\,]^2$, where n_s is the number of scattering centers and f is the scattering amplitude.

We assume that the spin splitting can be included by rewriting Eq. (7) as

$$\sigma_{xx}^{e}=\frac{2e^2\hbar}{\pi W m^*}\left[\,\phi-\tfrac{1}{2}\hbar\omega\,(1-\delta)\right] \quad , \tag{8}$$

where δ is the ratio of the spin splitting to the Landau-level separation.

This equation may be used to describe approximately the linear part of the falling conductivity plots in Fig. 9, but will fail at higher magnetic fields because of the neglect of nonparabolicity and collision broadening. If δ is known as a function of pressure or energy gap, the Fermi energy could be determined as a function of pressure by extrapolating the linear region of the plots to the field B_0 at which $\sigma_{xx}^{e}=0$, since $\phi=(\hbar eB_0/2m^*c)(1-\delta)$. Approximate values for ϕ at zero pressure have been obtained by taking $\delta=0.6$ from the data of Groves, Harman, and Pidgeon,[5] for a sample with $x=0.16$, and taking m^* as the band-edge effective mass, which is given by $m^*\simeq 3\hbar^2E_g/4P_K^2$.[1] Using the empirical relation[8] for E_g, the values for ϕ in samples 7B, 7B1, and 8B are, respectively, 9, 16, and 18 meV, which are consistent with values of E_F obtained above.

A similar magnetoresistance effect has been reported for BiSb alloys,[36] but in that case the electronic δ is greater than 1 and a semiconductor-to-semimetal transition is induced by a magnetic field.

The non-Ohmic effects (shown in Fig. 10) are similar to effects reported for n-type InSb, in which the carriers are "frozen out" onto donor impurities by the application of magnetic field.[37,38] We speculate that in our case the non-Ohmic effects involve the impact ionization of electrons from the acceptor level to the lowest-conduction-band Landau level.

The band-gap deformation potential D_G is related to the pressure coefficient by $D_G=\beta^{-1}dE_g/dP$, where β is the compressibility, $\beta=3/(c_{11}+2c_{12})$. Taking the value for dE_g/dP at 77 °K of 7×10^{-6} eV/bar, and values for the elastic constants interpolated between those for HgTe[39] and CdTe,[39] a value of 3.3 eV is obtained for the deformation potential.

SUMMARY

The dependence of the carrier concentration on pressure at 77 and 4.2 °K has been measured for p-type samples of $Hg_{1-x}Cd_xTe$ with x close to 0.14.

The results obtained at 77 °K for an annealed sample with low hole concentration can be described satisfactorily by the band model for the material and $\vec{k}\cdot\vec{p}$ theory. As-grown samples with high hole densities yielded values of np, too high to account for in this way, both at 77 and 4.2 °K. Analysis of the electron concentration as a function of pressure indicates that the Fermi-level position at 4.2 °K is situated at 20 and 16 meV above the valence band in the two as-grown samples, and 9 meV above the valence band in the annealed sample. In all cases, its position is independent of pressure. A model is proposed which required an acceptor level 9 meV above the valence-band edge in the annealed sample, with the Fermi level pinned by compensating donors. In the as-grown samples a band of levels at approximately 20 meV above the valence band is proposed, "metallic"-type impurity-band conduction taking place within this band.

A sharp transition is observed in the pressure dependence of both R and σ, which, according to our model, occurs at the pressure at which the conduction band passes through the acceptor level.

Magnetic freeze-out effects have been observed and attributed to the lowest-energy, spin-split, zero-order Landau level passing through the Fermi energy. Approximate values obtained for the Fermi energy agree with those given above.

ACKNOWLEDGMENTS

The authors thank Mary C. Finn for making the microprobe measurements of x and J. O. Dimmock, S. H. Groves, and A. J. Strauss for critically reading the manuscript.

APPENDIX: METHOD OF OBTAINING CARRIER DENSITIES AND MOBILITIES

Assuming a value of unity for the Hall scattering factor, the low-field Hall coefficient can be expressed as[26]

$$R(0) = -\frac{1}{e}\frac{nb^2 - p}{(nb+p)^2} \quad , \tag{A1}$$

where n and p are the electron and hole concentrations, respectively, and b is the electron-to-hole mobility ratio. Since b is greater than 100, $nb^2 \gg p$ for very low values of n/p and

$$R(0) \simeq -\frac{1}{e}\frac{nb^2}{(nb+p)^2} \quad . \tag{A2}$$

Expressing $R(0)$ in terms of the electron and hole contributions to the conductivity and rearranging gives

$$n = -\frac{1}{R(0)e}\left(1 + \frac{\sigma_p(0)}{\sigma_n(0)}\right)^{-2} \quad . \tag{A3}$$

The electron mobility can be expressed as

$$\mu_n = R(0)\,\sigma\,(0)\left(1 + \frac{\sigma_p(0)}{\sigma_n(0)}\right) \quad . \tag{A4}$$

The conductivity, in a magnetic field, can be expressed as

$$\sigma(B) = \frac{\sigma_n(B)\,\sigma_p(B)[R_n(B) + R_p(B)]^2}{\sigma_n(B)R_n(B)^2 + \sigma_p(B)R_p(B)^2} \quad , \tag{A5}$$

where $R_n(B)$ and $R_p(B)$ are the Hall coefficients which would be obtained if only the electrons or only the holes were present, and similarly $\sigma_n(B)$ and $\sigma_p(B)$ are the hole and electron transverse magnetoconductivities.

Because of the high values of b in $Hg_{1-x}Cd_xTe$, a range of fields exists for which $\mu B \gg 1$ and $\mu_p B \ll 1$. In this range, we can replace the coefficients for electrons in Eq. (A-5) by their saturation values and the coefficients for holes by their low-field values. Then

$$\sigma(B) = \frac{\sigma_n(\infty)\sigma_p(0)[R_n(\infty) + R_p(0)]^2}{\sigma_n(\infty)R_n(\infty)^2 + \sigma_p(0)R_p(0)^2} \simeq \sigma_p(0) \quad . \tag{A6}$$

The approximation is valid for our samples where $n \ll p$ and $b \gg 1$. Thus, $\sigma_p(0)$ can be obtained from the "saturation" value of $\sigma(B)$ (see Fig. 4). $\sigma_n(0)$ can be obtained from the conductivity in zero field, since

$$\sigma_n(0) = \sigma(0) - \sigma_p(0) \quad . \tag{A7}$$

Having determined $\sigma_p(0)$ and $\sigma_n(0)$, n may be obtained from Eq. (A3) and μ_n from Eq. (A4). When $\sigma_n(0) \gg \sigma_p(0)$, the method reduces to obtaining n directly as $1/R(0)e$ and μ_n as $R(0)\sigma(0)$. When $\sigma_n(0) \ll \sigma_p(0)$, the determination of n and μ_n becomes inaccurate.

p is obtained from the high-field Hall coefficient, since

$$p = 1/R(\infty)e + n \quad . \tag{A8}$$

For $n \ll p$

$$p \simeq 1/R(\infty)e \quad . \tag{A9}$$

The hole mobility μ_p is determined from

$$\mu_p = \sigma_p(0)/pe \quad . \tag{A10}$$

---

*Work sponsored in part by the Department of the Air Force. Some of the work was carried out at the Francis Bitter National Magnet Laboratory.

†Permanent address: Royal Radar Establishment, Malvern, Worcs., England.

[1]D. Long and J. L. Schmit, in *Semiconductors and Semimetals*, edited by R. K. Willardson and A. C. Beer (Academic, New York, 1970), Vol. 5, p. 175.

[2]T. C. Harman, in *Physics and Chemistry of II-VI Compounds*, edited by M. Aven and J. S. Prener (North-Holland, Amsterdam, 1967), p. 767; in *Proceedings of the International Conference on II-VI Semiconducting Compounds, Providence*, 1967, edited by D. G. Thomas (Benjamin, New York, 1967), p. 982.

[3]S. H. Groves and W. Paul, in *Proceedings of the International Conference on Semiconductor Physics* (Dunod, Paris, 1964), p. 41.

[4]E. O. Kane, in *Semiconductors and Semimetals*, edited by R. K. Willardson and A. C. Beer (Academic, New York, 1966), Vol. 1, p. 75; J. Phys. Chem. Solids 1, 249 (1957).

[5]S. H. Groves, T. C. Harman, and C. R. Pidgeon, Solid State Commun. 9, 451 (1971).

[6]T. C. Harman, W. H. Kleiner, A. J. Strauss, G. B. Wright, J. G. Mavroides, J. M. Honig, and D. H. Dickey, Solid State Commun. 2, 305 (1964).

[7]R. R. Galazka and T. Zakrewski, Phys. Status Solidi 23, K39 (1967).

[8]J. D. Wiley and R. N. Dexter, Phys. Rev. 181, 1181 (1969).

[9]R. A. Stradling and G. A. Antcliffe, J. Phys. Soc. Japan 21, S374 (1966).

[10]V. I. Ivanov-Omskii, B. T. Kolomiets, Yu. F. Markov, A. Sh. Mekhtiev, and K. P. Smekalova, Fiz. Tekh. Polnprov. 1, 1442 (1967) [Sov. Phys. Semicond. 1, 1203 (1967)].

[11]V. I. Ivanov-Omskii, B. T. Kolomiets, A. A. Markova, and A. Sh. Mekhtiev, Phys. Status Solidi 32, K83 (1969).

[12]W. Scott and R. J. Hager, J. Appl. Phys. 42, 803 (1970).

[13]C. T. Elliott and I. L. Spain, Solid State Commun. 8, 2063 (1970).

[14]C. T. Elliott, J. Phys. D 4, 697 (1971).

[15]S. Otmezguine, F. Raymond, G. Weill, and C. Vérié, in *Proceedings of the Tenth International Conference on the Physics of Semiconductors*, edited by S. P. Keller, J. C. Hensel, and F. Stern (U. S. Atomic Energy Commission, Cambridge, Mass., 1970), p. 536.

[16]R. Piotrzkowski, S. Porowski, Z. Dziuba, J. Ginter,

W. Giriat, and L. Sosnowski, Phys. Status Solidi 8, K135 (1965); R. Piotrzkowski and S. Porowski, in *Proceedings of the Tenth International Conference on II-VI Semiconducting Compounds, Providence*, 1967, edited by D. G. Thomas (Benjamin, New York, 1967), p. 1090.

[17]G. Weill and C. Vérié, Compt. Rend. 263, 463 (1966).

[18]C. Vérié and G. Martinez, Compt. Rend. 266, 720 (1968).

[19]T. C. Harman, MIT Lincoln Laboratory, Solid State Research Report No. 3, p. 2, 1970 (unpublished).

[20]A. G. Foyt (private communication).

[21]C. T. Elliott, Ivars Melngailis, T. C. Harman, and A. G. Foyt, J. Phys. Chem. Solids (to be published).

[22]John Melngailis, J. A. Kafalas, and T. C. Harman, J. Phys. Chem. Solids Suppl. 32, 407 (1971).

[23]I. L. Spain and S. Segall, Cryogenics 11, 26 (1971).

[24]J. S. Dugdale, in *Advances in High Pressure Research*, edited by R. S. Bradley (Academic, New York, 1969), Vol. 2, p. 105.

[25]W. S. Goree and T. A. Scott, J. Phys. Chem. Solids 27, 835 (1966).

[26]A. C. Beer, *Galvanomagnetic Effects in Semiconductors* (Academic, New York, 1963).

[27]D. J. Howarth, R. H. Jones, and E. H. Putley, Proc. Phys. Soc. (London) 70, 124 (1957).

[28]J. L. Schmit, J. Appl. Phys. 41, 2876 (1970).

[29]T. C. Harman and A. J. Strauss, J. Appl. Phys. 32, 2265 (1960).

[30]M. W. Scott, J. Appl. Phys. 40, 4077 (1969).

[31]G. W. Iseler, J. A. Kafalas, and A. J. Strauss, MIT Lincoln Laboratory, Solid State Research Report No. 2, p. 29, 1971 (unpublished).

[32]D. R. Scifres, N. Holonyak, Jr., C. B. Duke, G. G. Kleiman, A. B. Kunz, M. G. Crawford, W. O. Groves, and A. H. Herzog, Phys. Rev. Letters 27, 191 (1971).

[33]N. F. Mott, Rev. Mod. Phys. 40, 677 (1968); N. F. Mott and E. A. Davis, Phil. Mag. 17, 1269 (1968); N. F. Mott and W. D. Twose, Advan. Phys. 10, 107 (1961); N. F. Mott, Can. J. Phys. 34, 1356 (1956).

[34]C. T. Elliott, John Melngailis, T. C. Harman, and J. A. Kafalas, Bull. Am. Phys. Soc. 16, 401 (1971).

[35]R. Kubo, S. J. Miyake, and N. Hashitsume, in *Solid State Physics*, edited by F. Seitz and D. Turnbull (Academic, New York, 1965), Vol. 17, p. 361.

[36]N. B. Brandt, Y. A. Svistova, Yu. G. Kashirskiy, and L. V. Lyn'kov, Zh. Eksperim. i Teor. Fiz. 56, 65 (1969) [Sov. Phys. JETP 56, 35 (1969)], and references therein.

[37]E. H. Putley, in *Semiconductors and Semimetals*, edited by R. K. Willardson and A. C. Beer (Academic, New York, 1966), Vol. I, p. 289.

[38]H. Miyazawa, J. Phys. Soc. Japan 26, 700 (1969).

[39]G. Simmons and H. Wang, *Single Crystal Elastic Constants, A Handbook*, 2nd ed. (MIT Press, Cambridge, Mass., 1971).

PHYSICAL REVIEW B VOLUME 5, NUMBER 8 15 APRIL 1972

Thermal Brillouin Scattering in Cadmium Sulfide: Velocity and Attenuation of Sound; Acoustoelectric Effects*

A. S. Pine

Lincoln Laboratory, Massachusetts Institute of Technology, Lexington, Massachusetts 02173

(Received 17 May 1971)

The velocity and attenuation of 35-GHz longitudinal c-axis acoustic phonons have been measured as a function of temperature and free-carrier concentration by high-resolution Brillouin spectroscopy. These measurements determine both the acoustoelectric and the anharmonic contributions to the phonon damping for comparison to theoretical models.

I. INTRODUCTION

The velocity and attenuation of 35-GHz longitudinal c-axis hypersonic waves have been measured as a function of temperature between 100 and 400 °K in both high- and low-conductivity cadmium sulfide. Data are obtained by high-resolution thermal Brillouin spectroscopy employing tandem interferometer analysis of the back-scattered 6328-Å light. The acoustoelectric and the anharmonic contributions to the Brillouin linewidth—hence the acoustic attenuation—are distinguished by their dependence on temperature and electron cencentration. The anharmonic damping increases monotonically with temperature and is quite similar to that observed previously in α-quartz,[1] which is an insulator. This phonon-phonon interaction is compared to a recent theory by Niklasson[2] from which it is found that a single-relaxation-time approximation for thermal phonons poorly represents the data. The acoustoelectric damping, manifest as a low-temperature peak, is examined with an acoustic frequency on the order of the dielectric-relaxation and diffusion frequencies. Also, since the acoustic wavelength here is on the order of the electron mean free path, generalization of the low-frequency Hutson-White[3] acoustoelectric theory must be made. Diffusion effects play a significant role in this high-frequency study, so the results are sensitive to space-charge trapping. Furthermore